Biosensors and Bioelectronics 56 (2014) 137–143

Contents lists available at ScienceDirect

Biosensors and Bioelectronics

journal homepage: www.elsevier.com/locate/bios

Investigations of an electrochemical platform based on the layered MoS_2–graphene and horseradish peroxidase nanocomposite for direct electrochemistry and electrocatalysis

Haiyan Song [a,b], Yongnian Ni [a,b,*], Serge Kokot [c]

[a] State Key Laboratory of Food Science and Technology, Nanchang University, Nanchang 330047, China
[b] Department of Chemistry, Nanchang University, Nanchang 330031, China
[c] School of Chemistry, Physics and Mechanical Engineering, Queensland University of Technology, Brisbane 4001, Australia

ARTICLE INFO

Article history:
Received 9 November 2013
Received in revised form
2 January 2014
Accepted 4 January 2014
Available online 11 January 2014

Keywords:
MoS_2–graphene
Horseradish peroxidase
Layered nanocomposites
Electrocatalysis
Hydrogen peroxide

ABSTRACT

The self-assembly of layered molybdenum disulfide–graphene (MoS_2–Gr) and horseradish peroxidase (HRP) by electrostatic attraction into a novel hybrid nanomaterial (HRP–MoS_2–Gr) is reported. The properties of the MoS_2–Gr were characterized by X-ray diffraction (XRD), high-resolution transmission electron microscopy (TEM), electrochemical impedance spectroscopy (EIS) and cyclic voltammetry (CV). UV–vis and Fourier transform infrared spectroscopy (FT-IR) indicate that the native structure of the HRP is maintained after the assembly, implying good biocompatibility of MoS_2–Gr nanocomposite. Furthermore, the HRP–MoS_2–Gr composite is utilized as a biosensor, which displays electrocatalytic activity to hydrogen peroxide (H_2O_2) with high sensitivity (679.7 μA mM^{-1} cm^{-2}), wide linear range (0.2 μM–1.103 mM), low detection limit (0.049 μM), and fast amperometric response. In addition, the biosensor also exhibits strong anti-interference ability, satisfactory stability and reproducibility. These desirable electrochemical properties are attributed to the good biocompatibility and electron transport efficiency of the MoS_2–Gr composite, as well as the high loading of HRP. Therefore, this biosensor is potentially suitable for H_2O_2 analysis in environmental, pharmaceutical, food or industrial applications.

1. Introduction

The name, graphene (Gr), refers to carbon atoms densely packed into a single layer of a two-dimensional lattice. Since the isolation of Gr in 2004, it has been demonstrated that this substance has electronic properties that are suitable for many novel applications; also, it has a large surface area and high chemical tolerance (Zeng et al., 2010; Lin et al., 2012; Teymourian et al., 2013; Wang et al., 2013b). Consequently, the two-dimensional plane structure of Gr forms a platform for loading many different particles, and provides new pathways for the synthesis of functional nano-composites with different catalytic, magnetic, and optoelectronic properties (Shi et al., 2013; Chiu et al., 2013). In many nano-composites, there is a strong synergistic interaction between Gr and its composite components, which can greatly enhance the catalytic activity and stability (Zhang et al., 2010).

Molybdenum disulfide (MoS_2), a layered quasi-2 dimensional (2d) chalcogenide material (Sundaram et al., 2013) with a similar structure to graphite, is generally composed of three atomic layers: an Mo layer sandwiched between two S layers; such three layer stacks are held together by weak van der Waals interactions (Ma et al., 2013), and different types of atoms and molecules can be embedded precisely by intercalation methods (Huang et al., 2013). Thus, these kinds of material have found many applications, e.g. lithium batteries, catalysis, electrochemical devices and hydrogen storage (Kartick et al., 2013; Wang et al., 2013a; She et al., 2011; Lopez-Sanchez et al., 2013; Hu et al., 2012). Recently, the MoS_2–Gr hybrid system was successfully synthesized (Ma et al., 2011; Xiao et al., 2011; Shi et al., 2012; Wang et al., 2013c; Lin et al., 2013), and early results indicate that this material has good electron conductivity for electrochemical applications; in particular, it has been shown that this new material may be useful for dye-sensitive solar cell fabrication (Liu et al., 2012a), rechargeable Li^+ batteries (Chang and Chen, 2011a) and photocatalysis of H_2 (Xiang et al., 2012). Also, it is probable that this Gr–MoS_2 material will have at least similar properties and performance to materials containing composites involving the carbon-based materials with metal or metal oxide nano-particles (Su et al., 2013). Bio-nano-composites, which integrate natural biomolecules, hydrogels, or biopolymers with nano-materials, have been shown to have superior properties to those of their independent

* Corresponding author at: Department of Chemistry, Nanchang University, Nanchang 330031, China. Tel./fax: +86 791 83969500.
E-mail addresses: ynni@ncu.edu.cn (Y. Ni), s.kokot@qut.edu.au (S. Kokot).

0956-5663/$ - see front matter © 2014 Elsevier B.V. All rights reserved.
http://dx.doi.org/10.1016/j.bios.2014.01.014

components. Such nano-materials apparently are able to protect the activity of the redox proteins and enzymes (Song et al., 2013a; Choi et al., 2010; Chen et al., 2013).

In this work, a novel biosensor was constructed from the combination of MoS_2–graphene nano-material and horseradish peroxidase (HRP) enzyme, and it was demonstrated that this electrode is particularly suitable for the analysis of trace amounts of hydrogen peroxide.

Hydrogen peroxide, H_2O_2, is present in nature, particularly in waterways and various biological processes; also, it is commonly used in many chemical, pharmaceutical and clinical procedures, as well as in environmental, food manufacturing and industrial processes (Song et al., 2013b; Li et al., 2010). Typically, in such processes, H_2O_2 breaks down to produce molecular oxygen and highly reactive radicals, the desirable results of which, for example, are the bleaching of a textile fabric or cauterizing a wound, but if inappropriately applied, treatment with H_2O_2 can often produce severe damage of the substrate. Thus, analysis for H_2O_2 is generally important in chemical, biological and industrial samples. In this context, Gopalan et al. (2013) utilized the nano-diamond based sponges with entrapped horseradish peroxidase as an electrochemical probe to analyze H_2O_2. Satisfactory results were obtained in the linear concentration range of 1–45 mM and the limit of detection (LOD) was 59.0 μM. Yagati et al. (2013) developed an enzymatic biosensor based on the porous cerium dioxide, for the analysis of H_2O_2; much better results were obtained in the linear range of 0.2–3.0 mM, an LOD of 0.6 μM and a response time of 8 s as compared to those using other modified electrodes.

The aims of this work were as follows: 1) to prepare a novel nano-composite material, HRP–MoS_2–Gr; 2) to construct a new HRP–MoS_2–Gr/GCE (GCE—glassy carbon electrode) biosensor and investigate its electrochemical and electrocatalytic performances; and 3) to investigate the potential of this biosensor for quantitative analysis of H_2O_2 with the use of chronoamperometry.

2. Experimental

2.1. Reagents

Graphite powder, $NaMoO_4 \cdot H_2O$, and L-cysteine were purchased from Shanghai Chemical Reagent Co., Shanghai, China; horseradish peroxidase was obtained from Sigma-Aldrich Co., USA; hydrogen peroxide solution (30 wt% in H_2O); other reagents were purchased from Shanghai Chemical Reagent Co., Shanghai, China. Unless otherwise stated, the chemicals in this work were all reagents of Analytical Grade; they were used as received without further purification. Diluted H_2O_2 solution was freshly prepared before use. Phosphate buffer solution (PBS, 0.05 M, pH 7.44) was the supporting electrolyte, and was prepared from KH_2PO_4 and K_2HPO_4 salts. Double-distilled water was used throughout the experiments.

2.2. Instrumentation

UV–vis absorption spectra were recorded on an Agilent 8453 UV–vis spectrometer in the range of 200–800 nm (Agilent Technologies, Santa Clara, CA, USA). The FT-IR spectra were recorded from samples in KBr pellets with the use of a Thermo Nicolet 380 (Thermo Nicolet Co., USA). XRD (Bede DI System, UK) was used to investigate the MoS_2–graphene nano-composite (Cu Kα radiation ($\lambda = 1.5406$); Bragg angle range: 10–65°). The zeta potentials of MoS_2 – graphene aqueous dispersions were measured with the use of a zetasizer nano-system (Nano ZS, Malvern Instruments, UK). The structure of the samples was characterized by transmission electron microscopy, TEM (JEM-2010, JEOL Co., Japan).

All electrochemical experiments were performed on a CHI-660A electrochemical workstation (Shanghai Chenhua Apparatus Co., Shanghai, China) in conjunction with a standard three-electrode system: the working electrode—either the original or the modified GCE ($d = 3$ mm); the auxiliary electrode—a platinum wire, and the reference electrode—a saturated calomel electrode (SCE). A cell stand (Model BAS C1-A, USA) was used for voltammetric scanning and to stir the test solution during the experiment. The EIS experiments for the modified GCE were also performed in 5×10^{-3} mol L^{-1} $[Fe(CN)_6]^{-3/-4}$ (1:1) solution containing 0.1 mol L^{-1} KCl, with the use of a CHI-660A electrochemical workstation.

2.3. Synthesis of MoS_2–Gr composites

Graphene oxide (GO) was synthesized from natural graphite by Hummers and Offemans′ method with some minor modifications (Huang et al., 2013; Song et al., 2013a). The MoS_2–Gr composites were prepared in a solution, which was modified by the addition of L-cysteine (Chang and Chen, 2011b). GO (0.1 g) was poured into a 200 mL beaker with the addition of 50 mL double-distilled water. Then, 0.5 g $NaMoO_4 \cdot H_2O$ was added. After ultra-sonication and stirring for 30 min, pH of the solution was adjusted to 6.5 with 0.1 M NaOH. The mixture and L-cysteine (1.0 g) were dissolved in 100 mL double-distilled water and put into a 100 mL Teflon-lined stainless steel autoclave, sealed tightly, and heated at 180 °C for 36 h. After cooling in air, the black precipitate for each composite sample was collected by centrifugation, washed with double-distilled water and ethanol, and dried in a vacuum oven at 80 °C for 24 h.

2.4. Synthesis of HRP–MoS_2–Gr composites

The composite MoS_2–Gr (4.0 mg) powder was weighed accurately and dispersed in 2 mL double-distilled water for 1 h with the use of ultra-sonication. The obtained dispersion was mixed with 2 mL HRP (3.5 mg mL^{-1}). The mixture was sonicated in an ice–water bath for 15 min and then it was kept in this bath for 10 h with stirring. Subsequently, the dispersion was filtered through a nylon membrane (0.22 μm) to obtain the HRP–MoS_2–Gr. The composites were rinsed with double-distilled water three times, and dispersed in 1.0 mL double-distilled water. These samples were stored at 4 °C for further use.

2.5. Preparation of the differently modified GCEs

The glassy carbon electrode (GCE, $d = 3$ mm) was polished to a mirror-like shine with 0.1 and 0.05 μm alumina slurry sequentially, and then, it was sonicated in nitric acid (1:1), ethanol and double-distilled water, in turn. After the electrode was dried in air,

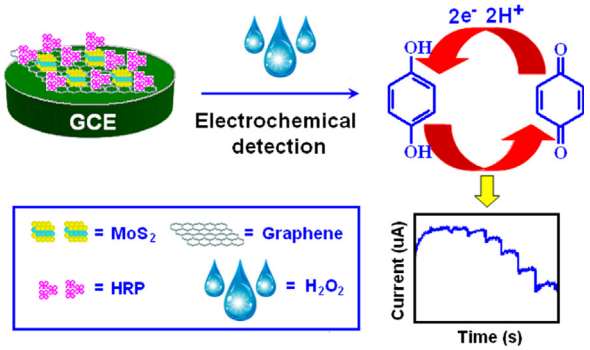

Fig. 1. The use of the HRP–MoS_2–Gr novel nano-composite biosensor for amperometric analysis of H_2O_2.

HRP–MoS_2–Gr dispersion (10 μL) was added dropwise onto the GCE and then dried at 4 °C in a refrigerator. Following this step, the 4% chitosan solution (5 μL) was deposited on the modified electrode and dried in air; this was carried out so as to improve the stability of the modified electrode. Other modified electrodes were similarly prepared using corresponding material dispersions.

The use of the HRP–MoS_2–Gr novel nano-composite biosensor for amperometric analysis of H_2O_2 is illustrated in Fig. 1.

3. Results and discussion

3.1. Characterization of the nano-composites

The graphene oxide mixture (Fig. 2A, Container a) prepared as described in Section 2.3 appears to be a brown solution with a touch of orange or red color; however, the color of the neighboring black MoS_2–Gr mixture is not transparent, which suggests the presence of fine particles (Fig. 2A, Container b). The TEM image (Fig. 2B) shows that a sheet of graphene oxide has a wrinkled and folded sheet structure; these structural elements may result from reaction sites at which oxidation occurred (Zeng et al., 2010). As shown in the TEM image of MoS_2 (Fig. S1, Supplementary material), this compound has flower-like morphology as well as some thinly folded layers, and when MoS_2 was combined with the graphene, similar dark flower-like matter appeared on the surface of the graphene sheet (Fig. 2C). These observations are consistent with the presence of layered MoS_2 on graphene.

XRD was also used to characterize the MoS_2–Gr nano-composites, and the five diffraction peaks (Fig. 2D), corresponding to the previously recorded (002), (100), (103), (105), and (110) planes of MoS_2 (Tang et al., 2013; Li et al., 2012); these observations confirmed that the MoS_2–Gr composites were prepared successfully.

The UV–vis spectra were used to demonstrate that the HRP–MoS_2–Gr has been successfully synthesized. As shown in Fig. 3A, the spectrum of the HRP solution (curve a) has a strong absorbance at 402 nm, which is in agreement with previous studies (Zhang et al., 2010; Li et al., 2010), and the MoS_2–Gr nano-material has no definitive MoS_2–Gr UV band (curve b). However, when the HRP–MoS_2–Gr composite is formed, a peak at 402 nm is observed (curve c). This peak is at exactly the same wavelength as the Soret band of the HRP, which suggests that this Soret band was unaffected during the formation of the HRP–MoS_2–Gr composite, i.e. the original structure of the immobilized HRP has not changed. Furthermore, supporting evidence for these observations was obtained from FT-IR measurements (Fig. 3B). Thus, the two

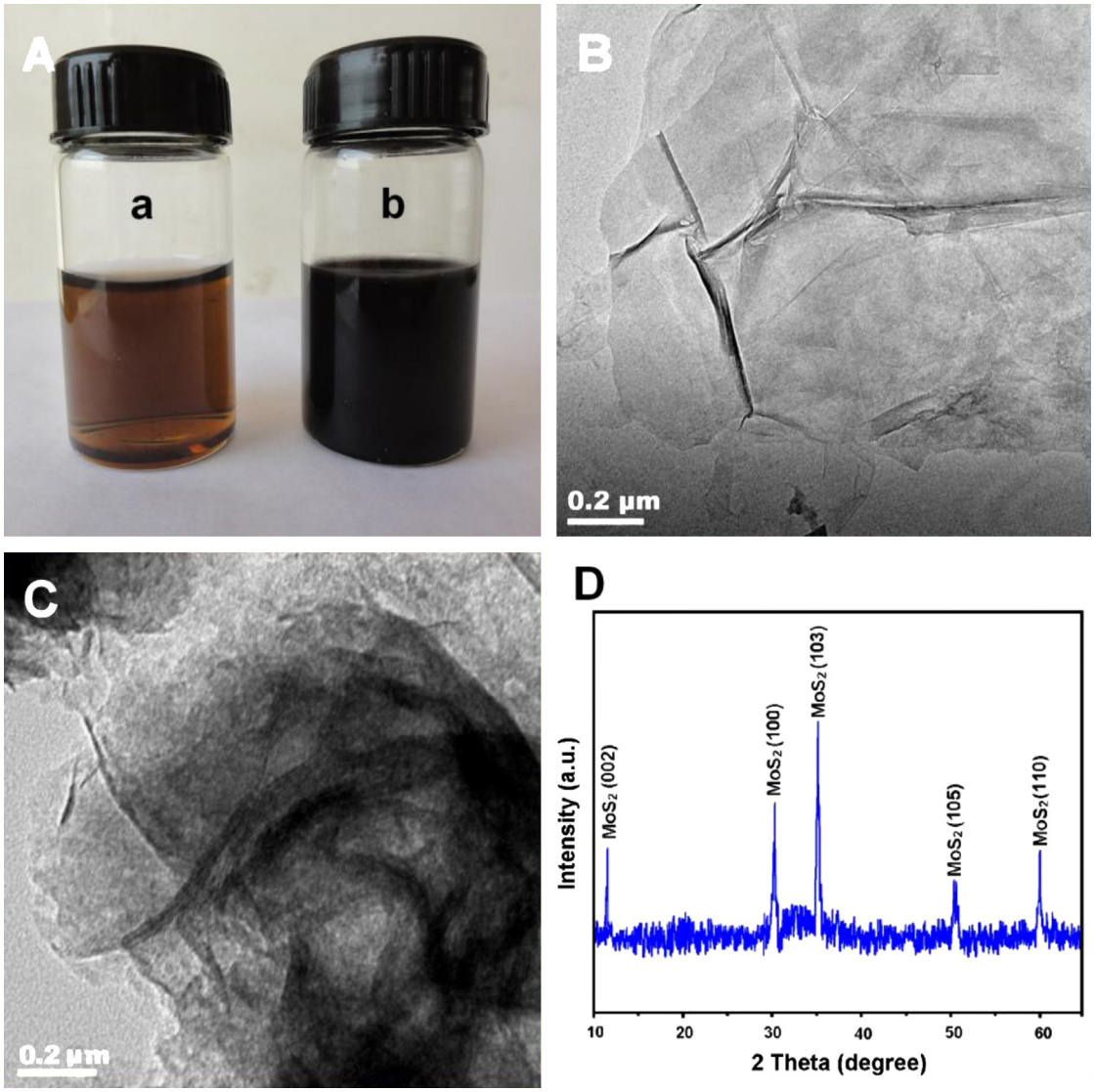

Fig. 2. Results from (A) photographic images of (a) graphene oxide (Gr) and (b) MoS_2–Gr; (B) TEM image of Gr; (C) TEM image of MoS_2–Gr and (D) XRD patterns of MoS_2–Gr.

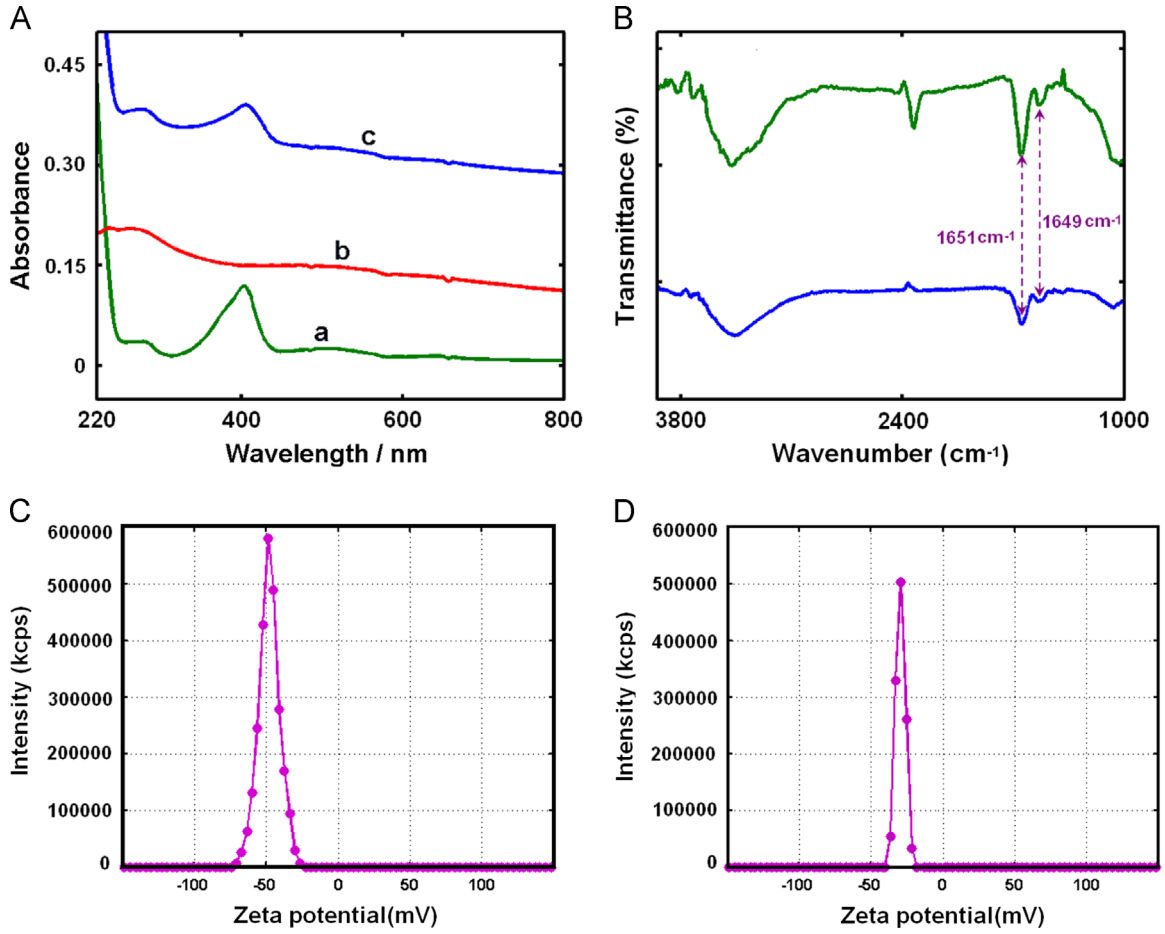

Fig. 3. (A) UV–vis absorption spectra: (a) HRP solution, (b) MoS_2–Gr suspension, and (c) HRP–MoS_2–Gr suspension; (B) FT-IR spectra: (a) HRP and (b) HRP–MoS_2–Gr nano-composites; (C) zeta potential curve of the MoS_2–Gr suspension in neutral aqueous solution; and (D) zeta potential curve of the HRP–MoS_2–Gr suspension in neutral aqueous solution.

characteristic bands of the free HRP, i.e. the amide I (1649 cm^{-1}) and II (1541 cm^{-1}) peaks (curve a), appear unchanged from those present in the spectrum of the HRP–MoS_2–Gr composite, i.e. the enzyme is immobilized and structurally unchanged (curve b). Consequently, MoS_2–Gr composite material appears to have good biocompatibility and facilitates the immobilization of enzymes.

As shown in Fig. 3C, the MoS_2–Gr nano-composites are negatively charged (zeta potential= −48 mV) in neutral aqueous solution; this indicates that this nano-composite has a similar negative charge to graphite oxide (zeta potential ~ −40 mV in neutral aqueous solution) (Ma et al., 2013). The HRP (PI=8.8) is positively charged in physiological media (Zeng et al., 2010). Thus, when the HRP solution is added to the MoS_2–Gr suspension, the two oppositely charged species should bind together via electrostatic attraction to form the HRP–MoS_2–Gr composite material, which is actually what was observed in practice. Thus, the zeta potential of the HRP–MoS_2–Gr suspension is about −34 mV (Fig. 3D), which indicates that this composite material also carries a negative charge under the same conditions. However, the value of the zeta potential is somewhat less than that of the MoS_2–Gr suspension. This lower potential could be attributed to the absorption of an enzyme with a positive charge, which ultimately lowers the surface charge of the composite material.

3.2. Electrochemical behavior of the modified electrodes

The electrochemical characterization of the electrode in its various states, GCE (a), HRP–MoS_2–Gr/GCE (b), and MoS_2–Gr/GCE (c) (Fig. 4, inset—curve 3), was carried out with the use of EIS and CV techniques (Fig. 4). EIS can provide important information about the interface properties of surface-modified electrodes. The semicircle diameter of the EIS plot at higher frequencies corresponds to the electron transfer-limited process, and the length of this diameter is proportional to electron-transfer resistance (Lin et al., 2013). As indicated in Fig. 4A, electron transfer resistance of the electrode decreases after its modification. It was clear that a big well-defined semi-circle at higher frequencies was obtained when the untreated GCE was used (curve a, Fig. 4A). Interestingly, when the GCE was covered by the MoS_2–Gr composite material, the corresponding semi-circle of the plot was reduced; this indicated that the MoS_2–Gr coating provides good conductivity (curve c, Fig. 4A). However, electron transfer capability of the modified electrode, HRP–MoS_2–Gr/GCE, was reduced in comparison with that of the MoS_2–Gr/GCE; this observation may be attributed to the presence of a hydrophobic layer on HRP, which prevented the interfacial electron transfer (Liu et al., 2012b), and this in turn, implied that the HRP was immobilized on the MoS_2–Gr (curve b, Fig. 4A). In addition, the Gr/GCE and MoS_2/GCE (inset, Fig. 4A, curve 1 and curve 2, respectively) were investigated, and it was found that the MoS_2–Gr/GCE has the least electron transfer resistance; this observation may be the result of a synergistic effect of MoS_2 and Gr, which demonstrated that MoS_2–Gr containing materials have high electron conductivities.

CV experiments with the same electrodes as noted above were also used to investigate any changes in electrode behavior with each different electrode, and the results were similar to those found with the EIS technique (Fig. 4B).

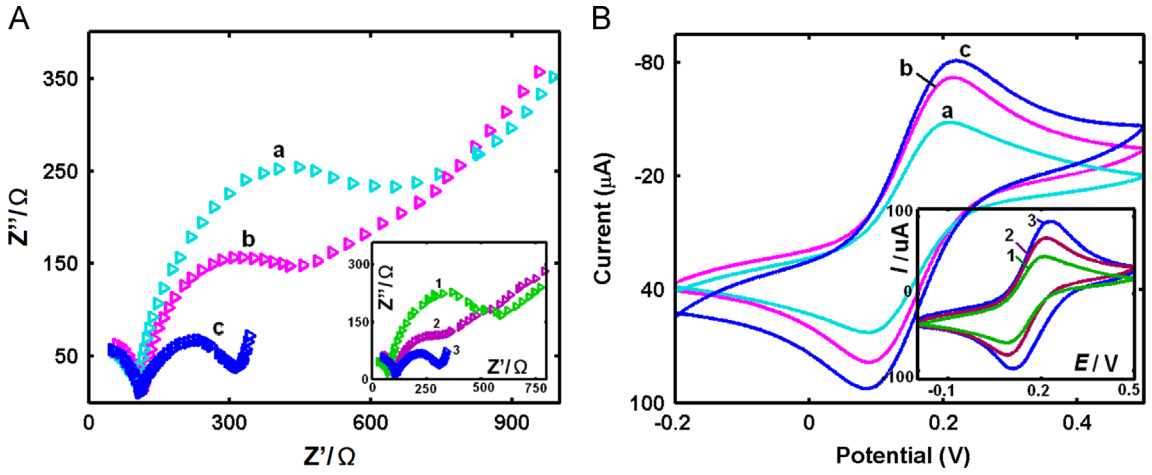

Fig. 4. Results from (A) electrochemical impedance spectroscopy (EIS), and (B) cyclic voltammograms (CVs) recorded at different electrodes in 1:15 mM $[Fe(CN)_6]^{-3/-4}$ in 0.1 M KCl solution. Curves: a. GCE, b. HRP–MoS_2–Gr/GCE, and c. MoS_2–Gr/GCE. Inset: 1. Gr, 2. MoS_2, and 3. MoS_2–Gr.

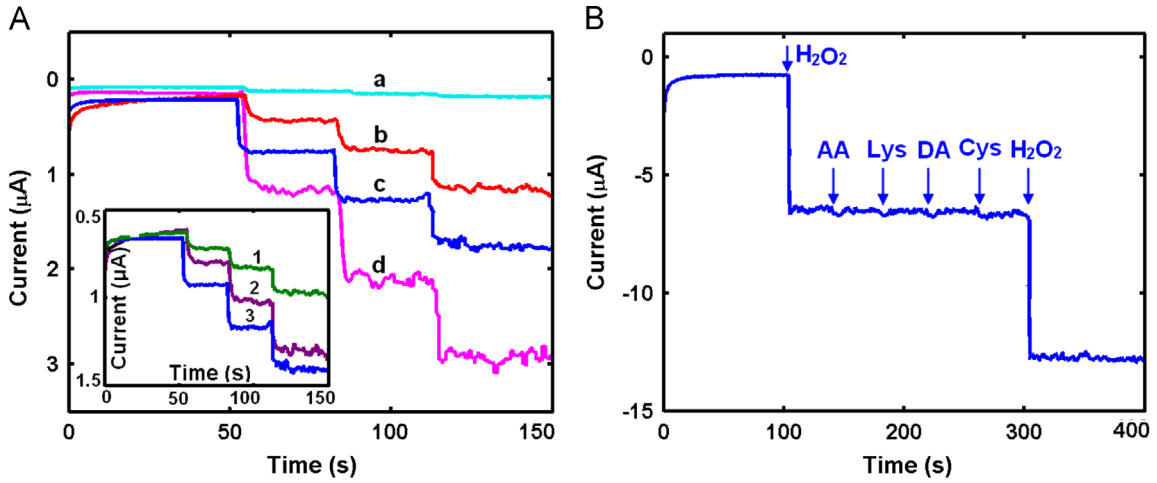

Fig. 5. (A) Amperometric response recorded at the HRP–MoS_2–Gr/GCE with successive addition of 10 μm H_2O_2. Curves: a. GCE, b. HRP, c. MoS_2–Gr, and d. HRP–MoS_2–Gr; inset: 1. Gr, 2. MoS_2, and 3. MoS_2–Gr. (B) Interference study with the use of successive additions of 0.04 mM H_2O_2, 1.0 mM ascorbic acid (AA), 1.0 mM dopamine (Lys), 1 mM cysteine (DA), 1.0 mM lysine (Cys), and 0.04 mM H_2O_2, in turn, to a stirred N_2-saturated aqueous solution of 0.05 M PBS (pH 7.44) containing 1.0 mM hydroquinone. Applied potential: −0.08 V (vs. SCE).

Chronocoulometric plots collected from the reduction of $K_3Fe(CN)_6$ (1.0 mM) in KCl (2.0 M) were obtained from the different electrodes used above so as to compare their apparent electrode areas. The relevant equation which enables the extraction of the area data is as follows (Huang et al., 2013):

$$Q = (2nFAD_0^{1/2}\pi^{-1/2}C_0)t^{1/2} \quad (1)$$

where Q denotes the absolute value of the reduction charge, n is the number of electrons transferred, F is a Faraday constant, A is apparent electrode area, t denotes time, and D_0 and C_0 are respectively, the diffusion coefficient and the bulk concentration of the oxidized form of the hexacyanoferrate (III) complex.

The apparent electrode area, A, may be estimated from the slope of the Q vs. $t^{1/2}$ plot (see Fig. S2A, Supplementary material). Thus, the order of the slope values was as follows: MoS_2–Gr/GCE > MoS_2/GCE > Gr/GCEI, i.e. the MoS_2–Gr/GCE has the largest value of A, and so this electrode shows the best electrochemical performance.

The cyclic voltammograms of an HRP–MoS_2–Gr/GCE in 0.05 M PBS (pH 7.44) in 1 mM hydroquinone were investigated at various scan rates. Well-characterized redox peaks of hydroquinone are observed at scan rates ranging from 10 to 190 mV s^{-1} (see Fig. S2B, Supplementary material). Both the oxidation and reduction peak currents increase with increasing scan rates, and also, the peak current is proportional to the square root of the scan rate (Fig. S2B, inset); this indicates the presence of typical diffusion-controlled electrochemical behavior.

3.3. Electrocatalysis of H_2O_2 at the HRP–MoS_2–Gr/GCE

The HRP–MoS_2–Gr/GCE showed high electrocatalytic activity towards the reduction of H_2O_2 in optimized conditions. PBS (pH 7.44) containing 1.0 mM hydroquinone was used as electrolyte. The above concentration of hydroquinone was selected by experiment (see Fig. S3A, Supplementary material) as demonstrated in the histogram of the catalytic current vs. concentration of hydroquinone (see Fig. S3B, Supplementary material). It was found that the strongest catalytic current occurred when the concentration of hydroquinone was 1.0 mM; hence, 1.0 mM hydroquinone was selected as optimum concentration for this work.

When H_2O_2 was added to the solution, the HRP immobilized on the HRP–MoS_2–Gr/GCE was oxidized and subsequently regenerated by the hydroquinone, which produced benzoquinone as the

reaction product. This benzoquinone is subsequently reduced, producing the current response of the biosensor. This current is proportional to the concentration of H_2O_2 and is closely related to the activity of the HRP. The reaction sequence of the catalytic process can be represented as follows (Camacho et al., 2007):

$$\text{HRP(Red)} + H_2O_2 \rightarrow \text{HRP(Ox)} + H_2O \quad (2)$$

$$\text{HRP(Ox)} + \text{hydroquinone} \rightarrow \text{HRP(Red)} + \text{benzoquinone} \quad (3)$$

$$\text{Benzoquinone} + 2e^- + 2H^+ \rightarrow \text{hydroquinone} \quad (4)$$

To investigate the performance of the different modified electrodes, amperometric experiments were conducted at each electrode, which was immersed in 0.05 M KH_2PO_4/K_2HPO_4 buffer (pH 7.44) containing 10 μm H_2O_2 and 1.0 mM hydroquinone; this solution was stirred and saturated with bubbling N_2 gas (Fig. 5A: GCE (curve a), HRP/GCE (curve b), MoS_2–Gr/GCE (curve c), and HRP–MoS_2–Gr/GCE (curve d)). The results indicated that the H_2O_2 reduction was barely present at the untreated GCE. However, the catalytic current at the HRP/GCE and also at the MoS_2–Gr/GCE significantly increased relative to that measured at the untreated GCE. This observation may reflect the strong catalytic effect of the MoS_2–Gr and the nature of the peroxidase of the HRP. A much larger current was observed at the HRP–MoS_2–Gr/GCE; this significant improvement could be attributed to the synergistic catalytic effect of HRP and MoS_2–Gr. In addition to these electrodes, the Gr/GCE (curve 1) and MoS_2/GCE (curve 2), were investigated as well (Fig. 5A, inset). The results indicated that the MoS_2–Gr/GCE (curve 3) has a much larger current response in the presence of the same H_2O_2 concentrations compared to the other two modified electrodes. This observation may be the result of a synergistic effect of MoS_2 and Gr.

Similar experiments were conducted at the HRP–MoS_2–Gr/GCE but different aliquots of H_2O_2 were added to the stirred electrolyte solution at −0.08 V (Fig. 6A). When the analyte was added to the electrochemical cell, a rapid increase in the reduction of current was observed; within 4 s this reached a level of 95% of the steady-state current. The current response increased linearly with the concentration of H_2O_2 in the range of 0.2 μm–1.103 mM (Fig. 6B), and this plot could be used as a calibration curve for the analysis of H_2O_2 at the modified electrode. The calibration equation was as follows: $I(\mu A) = 2.71 + 61.17c(\text{mM})$, with a correlation coefficient of 0.998. The sensitivity of the modified electrode was 679.7 μA mM^{-1} cm^{-2}, and the LOD was 0.049 μm with a signal-to-noise ratio of 3. When these results are compared with those from previous work, which involved the analysis of H_2O_2 (Gopalan et al., 2013; Yagati et al., 2013), the performance of the novel biosensor shows a significant improvement for both linear ranges and the LOD; these observations can be attributed to the high conductivity of the MoS_2–graphene, and the synergistic activity among MoS_2–graphene and HRP.

3.4. Selectivity and other properties of the modified electrode

In previous work (Song et al., 2013a), simultaneous electrooxidation of potential interferences such as ascorbic acid and cysteine was found to be a drawback for amperometric detection of the H_2O_2 analyte. In this work, the amperometric performance of the biosensor was investigated during the consecutive addition of 0.04 mM H_2O_2 and 1 mM interfering substances; the list of interfering substances included ascorbic acid (AA), lysine (Lys), dopamine (DA), and cysteine (Cys). It was evident from the traces of the response current that the influence of the tested interfering species on the response of the H_2O_2 was negligible (Fig. 5B); this observation indicated that the novel biosensor was highly selective for the analyte.

The reproducibility of the constructed biosensor was also researched. Thus, when four consecutive current measurements of a 0.1 mM H_2O_2 solution were recorded at the biosensor, the relative standard deviation (RSD) was ±3.2%. Similarly, when four separate electrodes were immersed into the above analyte solution under the same conditions, the RSD for electrode-to-electrode reproducibility was ±4.3%. In addition, the stability of the modified electrode as a function of time was studied for several weeks by the discontinuous measurement of the current responses from the reduction reaction of H_2O_2 while the biosensor was stored at 4 °C. There were no significant changes to the current response observed during the first 3 days. After the biosensor was stored for 2 weeks and then a month, it retained 91.5% and 84.2% of its original sensitivity, respectively. These results indicated that the stability of the electrodes and the reproducibility of the analysis of H_2O_2 were satisfactory; such performance was facilitated by the high levels of conductivity of the MoS_2–Gr, which actually did lead to an improved electron-transfer. In addition, the enlarged specific surface area of the MoS_2–Gr proved to be more conductive for the given loadings of the HRP.

4. Conclusions

The HRP–MoS_2–Gr nano-structures were prepared with the use of the common electrostatic self-assembly procedure, which involved the mixing of a solution of the negatively charged MoS_2–Gr with a

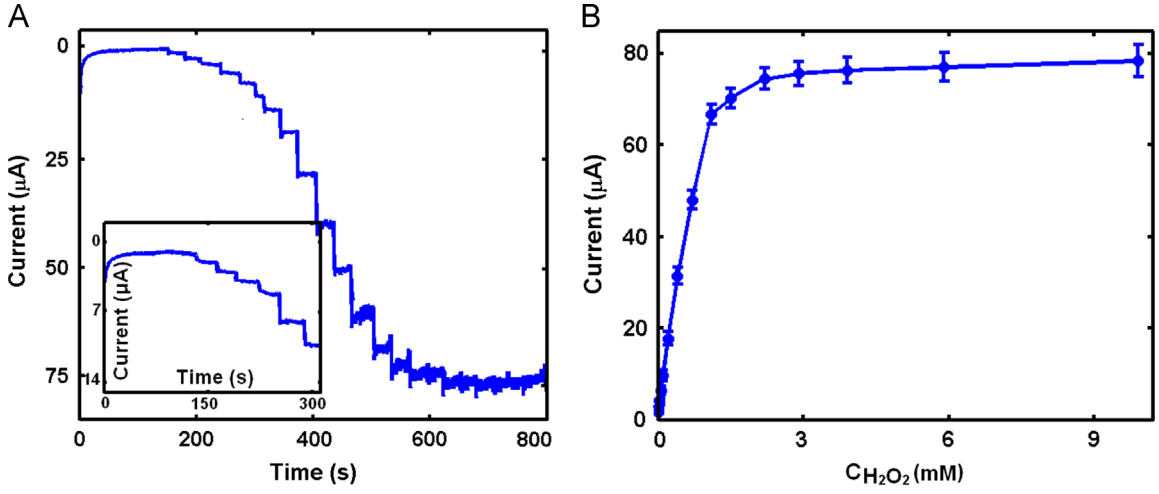

Fig. 6. (A) Amperometric response of the HRP–MoS_2–Gr/GCE with successive addition of H_2O_2 to a stirred N_2-saturated aqueous solution of 0.05 M PBS (pH 7.44). Applied potential: −0.08 V (vs. SCE). (Inset) Magnified plot of the small ladders. (B) Calibration curve of the HRP–MoS_2–Gr/GCE as a function of hydrogen peroxide concentration.

solution of the positively charged HRP under mild conditions. The obtained nano-composites were highly bio-compatible with the entrapped HRP, which maintained its native structure in the composites. In addition, the novel HRP–MoS_2–Gr/GCE biosensor performed particularly well during the electrocatalytic reduction of H_2O_2; thus, it had a fast response, a wide linear range, high sensitivity and stability. The successful strategy applied in this study suggested that the embedding of enzymes in the MoS_2–Gr nano-structure may pave the way in developing new solid support-enzyme nano-hybrids for the construction of novel biosensors.

Acknowledgments

The authors gratefully acknowledge the financial support of this study by the National Natural Science Foundation of China (NSFC-21065007), the Education Department Science Foundation of Jiangxi Province (GJJ-10037), the Graduate Student Innovation Program of Nanchang University (YC2013-S043), and the State Key Laboratory of Food Science and Technology of Nanchang University (SKLF-ZZA-201302 and SKLF-ZZB-201303).

Appendix A. Supporting information

Supplementary data associated with this article can be found in the online version at http://dx.doi.org/10.1016/j.bios.2014.01.014.

References

Camacho, C., Matias, J.C., Chico, B., Cao, R., Gomez, L., Simpson, B.K., Villalonga, R., 2007. Electroanalysis 19, 2538–2542.
Chang, K., Chen, W.X., 2011a. J. Mater. Chem. 21, 17175–17184.
Chang, K., Chen, W.X., 2011b. ACS Nano 5, 4720–4728.
Chen, H.C., Chen, Y.H., Chen, S.L., Chern, Y.T., Tsai, R.Y., Hua, M.Y., 2013. Biosens. Bioelectron. 15, 84–90.
Chiu, P.C., Su, R.Y.T., Yeh, J.Y., Yeh, C.Y., Tsiang, R.C.C., 2013. J. Nanosci. Nanotechnol. 6, 3910–3919.
Choi, K.S., Liu, F., Choi, J.S., Seo, T.S., 2010. Langmuir 15, 12902–12908.
Gopalan, A.L., Komathi, S., Anand, G.S., Lee, K.P., 2013. Biosens. Bioelectron. 46, 136–141.
Hu, T.C., Hu, L.T., Ding, Q., 2012. Surf. Coat. Technol. 24, 5060–5066.
Huang, K.J., Wang, L., Li, J., Liu, Y.M., 2013. Sens. Actuators B 178, 671–677.
Kartick, B., Suneel, K.S., Sourindra, M., 2013. Chem. Commun. 49, 1823–1825.
Li, N., Chai, Y.M., Dong, B., Liu, B., Guo, H.L., Liu, C.G., 2012. Mater. Lett. 88, 112–115.
Li, Q., Dong, X.C., Li, L.J., Hu, X., 2010. Talanta 82, 1344–1348.
Lin, J.Y., Chan, C.Y., Chou, S.W., 2013. Chem. Commun. 49, 1440–1442.
Lin, X.Y., Ni, Y.N., Kokot, S., 2012. J. Hazard. Mater. 243, 232–241.
Lin, X.Y., Ni, Y.N., Kokot, S., 2013. J. Hazard. Mater. 260, 508–517.
Liu, C.J., Tai, S.Y., Chou, S.W., Yu, Y.C., Chang, K.D., Wang, S.E., Chien, F.S.S., Lin, J.Y., Lin, T.W., 2012a. J. Mater. Chem. 22, 21057–21064.
Liu, Y., Liu, Y., Feng, H.B., Wu, Y.M., Joshi, L., Zeng, X.Q., Li, J.H., 2012b. Biosens. Bioelectron. 35, 63–68.
Lopez-Sanchez, O., Lembke, D., Kayci, M., Radenovic, A., Kis, A., 2013. Nat. Nanotechnol. 7, 497–501.
Ma, G.F., Peng, H., Mu, J.J., Huang, H.H., Zhou, X.Z., Lei, Z.Q., 2013. J. Power Sour. 299, 72–78.
Ma, Y.D., Dai, Y., Guo, M., Niu, C.W., 2011. Nanoscale 3, 3883–3887.
She, L., Li, J., Gu, D., Shi, Y.F., Che, R.C., Zhao, D.Y., 2011. Nanotechnology 22 (075702–075702).
Shi, X.Z., Gong, H., Li, Y.J., Wang, C., Cheng, L., Liu, Z., 2013. Biomaterials 20, 4786–4793.
Shi, Y.M., Zhou, W., Lu, A.Y., Fang, W.J., Lee, Y.H., Hsu, A.L., Kim, S.M., Kim, K.K., Yang, H.Y., Li, L.J., Idrobo, J.C., Kong, J., 2012. Nano Lett. 12, 2784–2791.
Song, H.Y., Ni, Y.N., Kokot, S., 2013a. Anal. Chim. Acta 25, 24–31.
Song, H.Y., Ni, Y.N., Kokot, S., 2013b. Microchim. Acta 180, 1263–1270.
Su, Y.Z., Zhang, Y., Zhuang, X.D., Li, S., Wu, D.Q., Zhang, F., Feng, X.L., 2013. Carbon 62, 296–301.
Sundaram, R.S., Engel, M., Lombardo, A., Krupke, R., Ferrari, A.C., Avouris, P., Steiner, M., 2013. Nano Lett.4, 1416–1421.
Tang, G.G., Wang, Y.J., Chen, W., Tang, H., Li, C.S., 2013. Mater. Lett. 100, 15–18.
Teymourian, H., Salimi, A., Khezrian, S., 2013. Biosens. Bioelectron. 15, 1–8.
Wang, J.Z., Lu, L., Lotya, M., Coleman, J.N., Chou, S.L., Liu, H.K., Minett, A.L., Chen, J., 2013a. Adv. Energy Mater. 6, 798–805.
Wang, X.Y., Gao, A., Lu, C.C., He, X.W., Yin, X.B., 2013b. Biosens. Bioelectron. 15, 120–125.
Wang, Z., Chen, T., Chen, W.X., Chang, K., Ma, L., Huang, G.C., Chen, D.Y., Lee, J.Y., 2013c. J. Mater. Chem. A 1, 2202–2210.
Xiang, Q.J., Yu, J.G., Jaroniec, M., 2012. J. Am. Chem. Soc. 134, 6575–6578.
Xiao, J., Wang, X.J., Yang, X.Q., Xun, S.D., Liu, G., Koech, P.K., Liu, J., Lemmon, J.P., 2011. Adv. Funct. Mater. 21, 2840–2846.
Yagati, A.K., Lee, T., Min, J., Choi, J.W., 2013. Biosens. Bioelectron. 47, 385–390.
Zeng, Q., Cheng, J.S., Tang, L.H., Liu, X.F., Liu, Y.Z., Li, J.H., Jiang, J.H., 2010. Adv. Funct. Mater. 20, 3366–3372.
Zhang, Q., Qiao, Y., Hao, F., Zhang, L., Wu, S.Y., Li, Y., Li, J.H., Song, X.M., 2010. Chem. Eur. J. 16, 8133–8139.